Ind. J. Pharm. Edu. Res., 2026; 60(3s):s1070-s1086.
https://www.ijper.org

Original Article

Cardioprotective Effect of Apigenin-Hydroxyapatite Nanocomposite against H_2O_2-Induced Injury in Cardiomyoblast Cells

Hafiz Makeen[1,*], Mohammad Albratty[2]

[1]Pharmacy Practice Research Unit, Department of Pharmacy Practice, College of Pharmacy, Jazan University, Jazan, SAUDI ARABIA.
[2]Department of Pharmaceutical Chemistry and Pharmacognosy, College of Pharmacy, Jazan University, Jazan, SAUDI ARABIA.

ABSTRACT

Background: Cardiovascular diseases remain the leading cause of mortality worldwide, largely driven by oxidative stress and inflammation during myocardial ischemia and reperfusion injury. Apigenin, a natural flavonoid, exhibits potent antioxidant and anti-inflammatory properties but suffers from poor solubility and bioavailability. To overcome these limitations, a novel Apigenin-Hydroxyapatite Nanocomposite (Api-HANPs) was developed to enhance its therapeutic efficacy against oxidative cardiac injury. **Materials and Methods:** Api-HANPs were synthesized via a green mechanochemical approach and characterized using FTIR, XRD, and FESEM analyses to confirm composite formation and structural morphology. The cardioprotective potential of Api-HANPs was evaluated in H9c2 cardiomyoblast cells exposed to Hydrogen Peroxide (H_2O_2)-induced oxidative stress. Cytotoxicity, antioxidant enzyme activities (SOD, CAT), lipid peroxidation (MDA), intracellular Reactive Oxygen Species (ROS) levels, apoptosis (AO/EB, DAPI), and mitochondrial membrane potential (Rh-123) were assessed. Molecular docking was performed to explore apigenin's binding affinity with the NF-κB protein, and immunofluorescence staining was used to evaluate NF-κB and Nrf2 nuclear translocation. **Results:** FTIR and XRD confirmed successful integration of apigenin into the hydroxyapatite matrix with altered crystallinity and improved surface morphology. Api-HANPs markedly improved cell viability in a dose-dependent manner, with maximal protection at 50 μM. Pretreatment with Api-HANPs significantly reduced H_2O_2-induced apoptosis, ROS production, and MDA levels while restoring antioxidant enzyme activity and mitochondrial membrane potential ($p < 0.0001$). Molecular docking revealed a strong binding affinity between apigenin and NF-κB (-7.7 kcal/mol), and immunostaining showed that Api-HANPs suppressed NF-κB nuclear translocation while promoting Nrf2 activation, indicating simultaneous anti-inflammatory and antioxidant actions. **Conclusion:** The Api-HANPs nanocomposite effectively mitigates oxidative stress-induced cardiomyoblast injury by restoring redox balance, preserving mitochondrial integrity, and modulating NF-κB/Nrf2 signaling pathways. These findings suggest Api-HANPs as a promising nanotherapeutic strategy for preventing oxidative cardiac damage and managing cardiovascular disorders.

Keywords: Apigenin, Cardiovascular Disease, Hydroxyapatite, Myocardial Injury, Cardiomyoblast.

Correspondence:
Dr. Hafiz Makeen
Pharmacy Practice Research Unit,
Department of Pharmacy Practice,
College of Pharmacy, Jazan University,
Jazan, SAUDI ARABIA.
Email: hafiz@jazanu.edu.sa
ORCID: 0000-0002-1078-2478

Received: 11-02-2026;
Revised: 05-03-2026;
Accepted: 28-04-2026.

INTRODUCTION

Globally, Cardiovascular Disease (CVD) causes 17.9 million people annually. Heart attacks, or Myocardial Infarction (MI), are devastating.[1,2] Durable ischemia, or inadequate blood supply, to a heart muscle segment causes cellular death (necrosis). Traditional therapies for MI often fall short due to the complex and multi-faceted pathophysiology, even though medicinal interventions such as beta-blockers, statins, and Angiotensin-Converting Enzyme (ACE) inhibitors have made great strides.[3] The condition is marked by a high mortality rate and significant long-term morbidity, often resulting in detrimental cardiac remodeling, diminished left ventricular function, and eventually, heart failure. The pathogenic cascade after MI entails significant and dynamic alterations in cellular metabolism, inflammation, and lipid profiles, underscoring the pressing need for more effective treatment options that may address various facets of the disease process.[4,5] Oxidative stress is a key contributor to cardiac damage. During a MI, the restoration of blood flow (reperfusion) to ischemic tissue, while essential for cellular survival, paradoxically induces a surge of ROS.[6] This Ischemia/Reperfusion (I/R) insult intensifies cellular damage by facilitating protein oxidation, lipid peroxidation, and DNA damage, potentially resulting in extensive cell death. The complex interaction between inflammation and oxidative stress creates a

DOI: 10.5530/ijper.20264260

detrimental loop that continues myocardial injury and hinders the heart's self-repair capacity. Therefore, there is an immediate necessity for bioactive systems that can concurrently eliminate reactive oxygen species and regulate inflammatory signals.[7,8]

Natural polyphenols, especially flavonoids, have garnered considerable interest due to their powerful, antioxidant, anti-inflammatory and cardioprotective properties.[9,10] The therapeutic efficacy of flavonoids has been extensively recorded in relation to diverse health ailments, including metabolic disorders, neurodegenerative illnesses, and hepatic toxicity.[11,12] Apigenin (4,5,7-trihydroxyflavone) emerges as a noteworthy prospect for medicinal advancement.[13,14] Previous studies indicate that apigenin may mitigate cardiac hypertrophy, represented by the swelling of heart muscle owing to stress, and provide protection against ischemia/reperfusion injury, a significant event in MI.[15] Its cardioprotective properties are ascribed to its capacity to regulate essential signaling pathways implicated in oxidative stress and inflammation. Apigenin demonstrates the capacity to neutralize free radicals, augment antioxidant enzyme activity, and inhibit pro-inflammatory cytokines, making it an effective agent against the harmful effects of ROS.[16-19] The clinical use of apigenin is significantly obstructed by its intrinsic physicochemical characteristics, notwithstanding its medicinal potential. Apigenin has limited solubility in biological fluids and inadequate bioavailability, indicating that only a little proportion of the molecule gets assimilated into the circulation and attains its target regions.[20,21]

To address these physicochemical constraints, this study employs a biomimetic strategy by incorporating apigenin into a mineral-based scaffold. Hydroxyapatite Nanoparticles (HANPs), an inorganic form of calcium phosphate, exhibit exceptional biocompatibility and mimic the natural mineral components of biological systems.[22-24] In contrast to synthetic delivery vehicles, the HANP scaffold serves as a structural stabilizer that preserves the bioactive molecule from degradation while improving its interaction with cellular membranes. We have created a stable Api-HANP by functionalizing HANPs with apigenin. This approach utilizes the nanoscale dimensions of the mineral matrix to enhance the stability and cellular uptake of apigenin, providing a synergistic platform for cardiac protection.

Despite the therapeutic characteristics of apigenin and HANP are well-documented, the effectiveness of a functionally integrated Api-HANP nanocomposite in a cardiac model has yet to be investigated. This research examines the cardioprotective efficacy of Api-HANPs against H_2O_2 induced oxidative stress in H9c2 cardiomyoblasts. We propose that this biomimetic platform offers enhanced protection by mitigating oxidative damage, preserving mitochondrial integrity, and inhibiting apoptotic pathways. In such an environment, HANP surpasses its traditional role as a passive carrier and acts as a biomimetic stabilizer that amplifies the inherent bioactivity of apigenin.[25] By creating a solid-state nanocomposite devoid of synthetic polymers or surfactants, we address the intrinsic limitations of free apigenin, namely its inadequate water stability and fast breakdown. The Api-HANP system functions as a cohesive substance, providing a persistent antioxidant defense against H_2O_2-induced damage. This association is especially efficacious in cardiomyoblasts, as the mineral scaffold provides enhanced biocompatibility relative to metallic or organic nano-carriers, which could potentially induce localized inflammation or secondary ROS.[26] Additionally, computational molecular docking and quantitative immunostaining were utilized to clarify the molecular connections between apigenin and the Nuclear Factor-kappa B (NF-κB) pathway, a principal regulator of the inflammatory cascade in cardiac damage. This work signifies a paradigm change from traditional drug delivery to the fabrication of bioactive nanocomposites, particularly designed to enhance cellular resilience against oxidative stress.

MATERIALS AND METHODS

Chemicals

Apigenin, calcium nitrate, liquid ammonia, phosphoric acid, and the fluorescent probes DCFDA, acridine orange, ethidium bromide, rhodamine 123, and DAPI were purchased from Sigma-Aldrich (USA). Gibco-Invitrogen (USA) supplied trypsin-EDTA, FBS, and DMEM-high glucose. All reagents and chemicals were of analytical grade and prepared freshly before each experiment.

Synthesis of HA nanoparticles

Initially, two distinct solutions were created. A 25 mL solution of 1 M $Ca(NO_3)_2$ and a 50 mL solution of 0.6 M Phosphoric acid (H_3PO_4) were prepared using DD water. The phosphoric acid solution was thereafter added dropwise to the calcium nitrate solution while maintaining continuous stirring. The pH of the resultant mixture was modified to 9 by the incorporation of liquid ammonia (NH_4OH). The mixture underwent ultrasonication for 5 min to achieve homogeneity. The subsequent mixer was placed in an autoclave (Teflon-lined SS) and imperilled to heating at 190°C for 240 min. The mixture was allowed to cool to Room Temperature (RT), and the white residue was collected by centrifuging it at 3500 rpm for 10 min. The precipitate was washed three times: first, it was rinsed with ethanol to get rid of organic contaminants, and then it was washed twice with DD water to get rid of any leftover ions. After that, the mixture was dried in a 90°C oven for one day to get pure HA nanoparticle powder.

Preparation of Api-HANPs nanocomposite

The Api-HANP nanocomposite was created using a solid-state mechanochemical method. In summary, 100 mg of apigenin and 100 mg of hydroxyapatite nanoparticles (1:1 w/w ratio) were precisely measured and placed into a stainless steel ball

mill chamber. The materials underwent dry milling for 2 hr at 800 rpm. This anhydrous mechanochemical method enabled the high-energy collision of particles, enhancing the surface functionalization of the HANPs with apigenin without employing organic solvents. Subsequent to the milling process, the resulting stabilized nanocomposite was retrieved and preserved at 4°C for future characterisation and biological evaluations. The Polydispersity Index (PDI) of the Api-HANP nanocomposite was ascertained using Dynamic Light Scattering (DLS) utilizing a Malvern Zetasizer Nano ZS. Samples were diluted in deionized water and subjected to sonication for 5 minutes to achieve uniform dispersion. Measurements were conducted at 25°C with a detection angle of 173°. Three independent measurements (10-15 runs each) were performed for each sample.

Physicochemical characterization

The fabricated nanocomposite product was characterized in different ways. FTIR spectrum from 4000 to 400 cm^{-1} was obtained using a Cary-660 spectrophotometer to detect functional groups. XRD analysis was conducted on the crystal structure and phase purity using a D8 Advance diffractometer. Surface morphology and microstructure were examined using a Carl Zeiss FESEM, with samples coated in gold or platinum to avoid charging.

Cell Culture

H9c2 rat cardiomyoblast cells were procured from the National Centre for Cell Science (NCCS) in Pune, India. The cells were grown in Dulbecco's Modified Eagle Medium (DMEM) enriched with 10% Fetal Bovine Serum (FBS) and 1% antibiotic-antimycotic solution in a humidified environment containing 5% CO_2 at 37°C. All tests were conducted with cells between passages 5 and 12 to guarantee phenotypic uniformity and metabolic stability. Cells were sub-cultured at 70-80% confluence to avert spontaneous differentiation, as elevated passage numbers have been documented to demonstrate modified responses to toxic stimuli and variations in myogenic markers. For the tests, cells were inoculated at a density of 5×10^4 cells/well (24-well plates), with each well holding 1 mL of media, and were subjected to treatment after 3 days of growth.

Treatment protocol

The cells were pre-treated with different doses of Api-HANPs (5 to 100 µM) over a duration of 24 hr. Subsequently, the cells were rinsed with PBS, and cardiac damage was induced using hydrogen peroxide (250 µM) for 60 min.

Vitamin C (100 µM) was employed as a standardized positive control to assess the antioxidant and cytoprotective efficiency of the synthesized Api-HANP nanocomposite in all biological assessments. All assays, including cell viability (MTT), nuclear morphology (DAPI and AO/EtBr staining), Mitochondrial Membrane Potential (MMP), and intracellular Reactive Oxygen Species (ROS) accumulation, involved pre-treatment of H9c2 cardiomyoblasts with Vitamin C for 2 hr before the induction of oxidative stress using H_2O_2 (250 µM). This group acted as a comparative standard to assess the efficacy of the Api-HANP platform in neutralizing oxidative damage, maintaining mitochondrial integrity, and inhibiting programmed cell death. All comparison treatments were conducted under uniform experimental circumstances to guarantee statistical and biological integrity.

MTT Assay

Cell viability was measured using the MTT test. After being exposed to varied doses of Api-HANP (5-100 µM) over 24 hr, H9c2 cells were treated with 250 µM H_2O_2 for 1 hr. The MTT experiments demonstrated that Api-HANP doses between 5 -100 µM did not significantly influence the viability of H9c2 cells; hence, this range was chosen to assess the dose-dependent cardioprotective effects against H_2O_2. The next step was to treat the cells with a 1 mg/mL MTT solution for three hours at 37°C. Using a Mindray MR-96 microplate reader, the absorbance was measured at 570 nm after dissolving the formazan product in 100 µL of DMSO.

Assessment of apoptosis using AO/EB staining

A PBS washing was performed on the cells after treatment. An AO/EB staining solution was prepared by mixing 50 µg/mL of acridine orange with 50 µg/mL of ethidium bromide in an equivalent amount. A total of 100 µL of staining solution was added to the cells, and they were left to incubate at RT without light for 20 min. The cells were then cultured on glass slides and seen using a 480 nm excitation filter-equipped Olympus CKX53 fluorescence microscope.

Protein Extraction and Quantification

Cells were lysed using a cold lysis buffer, followed by sonication on ice. Sonication on ice was followed by centrifugation at 12,000 x g for 15 min at 4°C. The Bradford test, with BSA serving as the standard, was used to quantify the protein content in the cell lysate.

Antioxidant Enzyme Assays

Antioxidant enzyme activity and lipid peroxidation levels were evaluated in cell lysates utilizing standard techniques with slight changes. Subsequent to treatment, cells were collected, rinsed twice with ice-cold PBS (pH 7.4), and lysed in ice-cold lysis buffer; the lysates were then centrifuged at 12,000 × g for 15 min at 4°C, with the supernatant obtained for analysis. Catalase (CAT) activity was measured utilizing the Catalase Assay Kit (ELABSCIENCE, E-BC-K031-M), while Superoxide Dismutase (SOD) activity was assessed using the Superoxide Dismutase Assay Kit (ELABSCIENCE, E-BC-K020-M), following the manufacturer's guidelines and the methodology of Aicha *et al.*,[27] with absorbance recorded at 450 nm on a microplate reader.

Lipid peroxidation was assessed by measuring Malondialdehyde (MDA) levels using the TBARS Assay Kit (ELABSCIENCE, E-BC-K025-M):[28] reaction mixtures were incubated at 95-100°C for 15-30 min, subsequently cooled to room temperature, centrifuged to eliminate precipitates, and absorbance was measured at 532 nm using a spectrophotometer. Assays were performed in three separate biological replicates (n = 3), each including technical triplicates; enzyme activity and MDA levels were adjusted to total protein (Bradford assay) and presented as Mean ± SD.

ROS staining

H9c2 cells were treated with Api-HANPs at five different concentrations-for 24 hr. After that, oxidative stress was induced by exposure to 250 µM H_2O_2 for 1 hr. The cells were then washed with cold PBS and incubated with 50 µM DCFH-DA at 37°C for 30 min in the dark. After incubation, the cells were washed twice with PBS, and fluorescence images were captured using a fluorescence microscope (CKX53, Olympus, Japan) with excitation and emission wavelengths of 488 nm and 530 nm. Intracellular ROS levels were quantified by measuring the Mean Fluorescence Intensity (MFI).

Mitochondrial Membrane Potential Assessment

The cells were first treated, and then incubated with 100 µL of a Rh123 staining solution containing 10 mg/mL. The mixture was then incubated for 20 min at 37°C in the dark. Fluorescence intensity was measured using a fluorescence microscope (CKX53, Olympus, Japan) after two rinses with PBS. Decreases in the intensity of Rh123 fluorescence are indicative of decreases in mitochondrial membrane potential (ΔΨm).

Nuclear staining with DAPI

In order to evaluate the structure of the nucleus, the cells were treated with a 3.7% formaldehyde solution for a duration of 10 minutes at room temperature. This was then followed by three rinses using PBS. The cells were subsequently permeabilized using a 0.2% Triton X-100 for a duration of 5 minutes, followed by another round of washing with PBS. Afterwards, the cells were treated with DAPI (5 µg/mL) and incubated for 10 minutes in the absence of light. Following the removal of excess DAPI through PBS washing, nuclear morphology was examined using a fluorescence microscope (CKX53, Olympus, Japan) with excitation and emission wavelengths of 358 nm and 461 nm, respectively. The fluorescence intensity of Rh123 is indicative of a decrease in mitochondrial membrane potential (ΔΨm).

Molecular docking analysis

A potential binding mechanism between Apigenin and NFκB was examined by a molecular docking study. Initially, we acquired the three-dimensional configurations of Apigenin (PubChem CID: 5280443) from the PubChem database (https://pubchem.ncbi.nlm.nih.gov/). Subsequently, we obtained the three-dimensional configuration of the I-Kappa-B-Alpha/NF-Kappa-B Complex with the Protein Data Bank identification number (PDB ID - 1NFI). Ultimately, we employed AutoDock (version 15.7, MGL Tools) to simulate the interaction between Apigenin and a protein that plays a role in the NF-kB pathway. Autodock is a computational software that predicts the compatibility between a medicine molecule and a protein molecule, determining their ability to create a stable link. It calculates the binding energy, which quantifies the strength of the attraction between the two molecules. Autodock indicates a more favourable interaction between the protein and the ligand by assigning a lower binding energy value. When the score is negative, it means that the predicted fit is quite accurate. For the same reason that lighting a match releases energy, bonding usually does the same. A negative number is used to represent this released energy in the calculations.

Immunofluorescent staining assay

To examine the effects of Api-HANPs on oxidative stress and inflammation, H9C2 cells were cultured in a humidified chamber at 37°C with 5% CO_2. The cells were randomly divided into three groups for the experiment after they achieved 80% confluence. The comparison group did not get any therapy. To induce oxidative stress and inflammation, the H_2O_2 group was exposed to 250 µM H_2O_2 for a duration of 1 hr. The Api-HANPs group was pretreated with 5 µg/mL of Api-HANPs for 24 hr, followed by exposure to 250 µM H_2O_2 for 1 hr. In order to fix the cells, they were exposed to 4% paraformaldehyde for 15 min at room temperature after each treatment. After that, they were incubated with 0.1% Triton X-100 for ten minutes, and then 5% BSA was used to block them for an hour. Next, NF-κB p65 (1:400) and Nrf2 (1:200) primary antibodies were used. For the next day, the cells were allowed to remain at 4°C. Secondary antibodies labelled with Alexa Fluor 488 and 594 were then added to the cells after washing and left to sit in a dark chamber at room temperature for 1 hr. A fluorescent microscope was used to observe and quantify the entry of NF-κB p65 and Nrf2 into the nucleus after the nuclei were stained with DAPI.

Statistical analysis

Statistical analysis was performed on data obtained from three distinct experiments. Data are presented as the Mean ± Standard Deviation (SD) or Standard Error of the Mean (SEM), as appropriate. Group comparisons were assessed utilizing repeated measures ANOVA or Student's t-test, contingent upon the experimental design. Statistical analyses were performed utilizing GraphPad Prism software (version 8, San Diego, CA, USA), with statistical significance defined at $p < 0.05$. The figures denote specific p-values indicated by asterisks: $^{*}p < 0.05$ (if relevant, albeit not expressly mentioned in the text), $^{**}p < 0.01$, $^{***}p < 0.001$, and $^{****}p < 0.0001$. # denotes a comparison between the control and

treated groups, while * signifies a comparison between the treated and other experimental groups.

RESULTS

Physicochemical analysis

Figure 1a shows the FTIR spectra of pure Apigenin, pure HANPs, and Api- HANPs nanocomposite. In the spectrum of pure HANPs, Phosphate (PO_4^{3-}) vibrations dominate, with asymmetric stretching peaks at 1097 and 1028 cm^{-1}, symmetric stretching peaks at 951 cm^{-1}, and a split asymmetric bending band at 563 and 604 cm^{-1}. The large peak at 3424 cm^{-1} and the tiny peak at 1620 cm^{-1} represent the hydroxyl group stretching and bending vibrations of adsorbed water molecules.[29] The spectra of pure Apigenin exhibits peaks (C=O) at 1648 cm^{-1}, 1620 cm^{-1} (C=C), and a wide band about 3300 cm−1 (O-H).[30] The Api-HANPs nanocomposite's FTIR spectrum shows that Apigenin was successfully incorporated onto HANPs nanoparticles. The nanocomposite spectrum shows Apigenin and HANPs peaks, with HANPs phosphate bands at 1069, 1026, 946, 558 and 602 cm^{-1}. Importantly, the primary phosphate peaks shift somewhat from pure HANPs. In the nanocomposite, the peak at 1028 cm^{-1} in pure HANPs moves to 1026 cm^{-1}, and the band at 1097 cm^{-1} shifts to 1069 cm^{-1}. In the nanocomposite, Apigenin's C=O band at 1648 cm^{-1} moves to 1640 cm^{-1}. This slight but considerable peak change suggests hydrogen bonding or electrostatic interactions between organic Apigenin molecules and the inorganic HANPs surface.[31,32] Similar spectrum shifts indicate effective composite synthesis and molecular interaction, as reported by Sysak *et al.*[33]

The XRD patterns of pure HANPs and the Api-HANPs exhibit different features essential for evaluating the material's crystalline structure. The diffraction peaks for pure HANPs (Figure 1b) are distinct and crisp, reflecting its extremely crystalline characteristics. The most distinctive peaks of HANPs are often seen at two theta values of 25.91°, 31.95°, and 32.50°, conforming to the (002), (211), and (300) crystallographic planes, respectively.[34] The peak at 31.95° ((211) plane) is notably pronounced and serves as a critical indication of the HANPs phase. Conversely, the XRD pattern of the Api-HANPs nanocomposite displays larger and less strong peaks. The widening and diminished intensity indicate a decline in the crystallinity of the HANPs component. The principal HANPs peaks at 2θ values of 25.91°, 31.95°, and 32.50° remain evident, but with less sharpness, attributable to the effective integration of apigenin into the HANPs lattice.[35] The amorphous characteristics of apigenin, together with its interaction with the HANPs surface, disturb the long-range ordering of HANPs nanocrystals, resulting in the observed peak widening. This structural alteration serves as a crucial indicator of successful nanocomposite formation and has been documented in analogous studies, including that of Manzoor *et al.* (2025), which synthesized drug-loaded HANPs nanoparticles for biomedical applications, observing comparable variations in XRD patterns following drug incorporation.[36] The alteration in crystallinity is often advantageous for drug delivery applications, as the increased surface area and reduced crystal size may improve drug loading and release efficacy, which is especially pertinent for cardiomyoblast protection.

The Scherrer equation was utilized to quantitatively estimate the primary crystallite size, focusing on the significant (002) diffraction peak at around 2θ= 25.8, indicative of the c-axis development of HA crystals. The Scherrer equation is articulated as:

$$D=K\lambda/\beta\cos\theta \quad (1)$$

In this expression, K signifies a dimensionless shape factor, whereas λ indicates the X-ray wavelength of the CuKα radiation (0.154 nm). The parameter β is the Full Width at Half Maximum (FWHM) of the most prominent diffraction peak, notably the (211) reflection, expressed in radians to accommodate line broadening, and θ denotes the Bragg angle corresponding to the peak point. The mean crystallite size, derived from the diffraction peak at the (211) plane, was found to be 17.26 nm for pure HA and 17.29 nm for the Api-HANP nanocomposite. The slight increment in the crystallite size of Api-HANP indicates the effective incorporation of Apigenin into the mineral matrix, potentially affecting lattice strain and overall particle development while preserving the core HA phase.

The FESEM findings in Figure 1c reveal important morphological changes in produced materials. HANPs shows with a rod-like shape and homogeneous nanoscale dispersion. Numerous investigations on biomedical HANPs synthesis have documented this shape.[37] Api-HANPs have a heterogeneous shape with rod-like and spherical features. HANPs nanorods have incorporated and distributed apigenin, as seen by this morphological alteration. Apigenin affects HANPs self-assembly and crystallization, creating a composite material with a more complex surface topography. The FESEM photographs were analyzed quantitatively using ImageJ software to determine the particle size distribution. The findings indicated that the synthesized Api-HANP displayed a very homogeneous distribution, with sizes between 90 and 200 nm. The heterogeneous structure's enhanced surface roughness and various binding sites may improve medication loading and controlled release. As shown in comparable drug-delivery methods for cardiac tissue engineering, persistent apigenin release is essential for cardiomyoblast protectivity to offer an antioxidant and anti-inflammatory impact.

The size uniformity of the Api-HANP nanocomposites were assessed using the Polydispersity Index (PDI) (Figure 1d). The Api-HANP nanocomposites demonstrated a PDI value of 0.123, signifying a narrow size distribution and a high level of homogeneity within the solution. PDI values below 0.2 indicate a monodisperse population, implying that the incorporation of Apigenin into the HA mineral matrix did not result in notable

agglomeration or structural heterogeneity. The low PDI value is essential for guaranteeing uniform cellular uptake and consistent biological responses in the cardiomyoblast damage model.

Preliminary Assessment of H_2O_2-treated, Pristine HANPs and Pure Apigenin

To establish a suitable model for oxidative stress, H9c2 cells were exposed to varying concentrations of H_2O_2. Our findings revealed a substantial decrease in cell viability at 250 µM H_2O_2, demonstrating its effectiveness in inducing oxidative damage (Figures 2a, 2b). This concentration was therefore selected for subsequent experiments.

To determine the safety profile of the various components, H9c2 cells were subjected to different concentrations (5-100 µM) of pure Apigenin and pristine HANPs (Figures 3 and 4). The MTT assay results indicated that both compounds had minimal cytotoxicity, with cell viability consistently exceeding 90% throughout the entire concentration range. The superior biocompatibility of the HANP scaffold corresponds with its characteristics as a

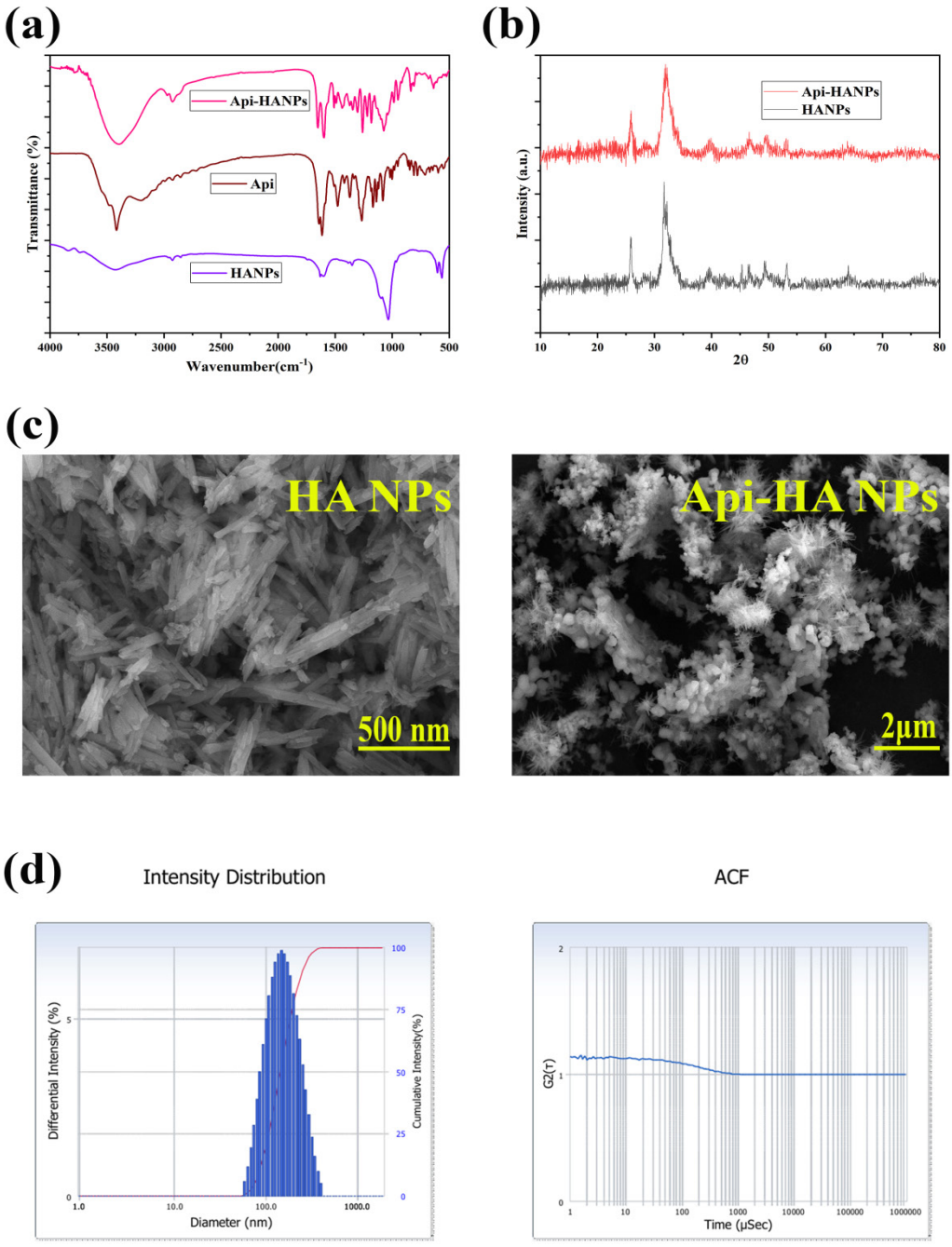

Figure 1: (a) FTIR spectrum Pure Api, pure HANPs and Api-HANPs nanocomposite; (b) XRD pattern of pure HANPs and Api-HANPs nanocomposite; (c) FESEM images of pure HANPs and Api-HANPs nanocomposite; (d) Polydispersity Index (PDI) of the Api-HANP nanocomposite, indicating a monodisperse population with a PDI of 0.123.

biomimetic calcium phosphate mineral, emulating the inorganic composition of living tissues. Likewise, pure Apigenin, a naturally occurring dietary flavonoid, exhibited no detrimental effects on cardiomyoblast viability under the examined conditions. The absence of intrinsic toxicity in both the bioactive chemical and the mineral carrier indicates that any biological alterations detected in following tests stem from therapeutic signaling rather than stress generated by the materials.

Cytoprotecting effect of Api-HANPs against H2O2-induced H9c2 cells

The chosen concentrations of Api-HANP therapy (5, 25, 50, and 100 µM) were determined by preliminary cytotoxicity evaluations and recognized pharmacological ranges for flavonoids in cardiac cell models. An MTT cell viability assay was performed to assess the safety of the Api-HANP; H9c2 cells exposed to Api-HANPs at concentrations up to 100 µM exhibited a cell viability, so affirming the excellent biocompatibility of the HA NP scaffold. The concentration range was substantiated by existing literature, indicating that low doses of Apigenin (5-20 µM) can activate antioxidant signaling, whereas higher concentrations (up to 100 µM) are typically required to elicit a notable protective effect against severe oxidative damage, such as that induced by H_2O_2.[38,39] By employing this extensive range, we assessed the dose-dependent performance of the nanocomposite and identified the optimal concentration necessary to regulate the cardiomyoblast microenvironment without triggering pro-oxidant effects.

H9c2 cells were exposed to H_2O_2 following pretreatment with different concentrations of Api-HANPs and a positive control group (H_2O_2+Vit C) to assess their cytoprotective properties (Figure 5a). In comparison to the H2O2-treated damage group, there was a substantial dose-dependent enhancement in cell viability ($p < 0.0001$) in the Api-HANP treated cells. The restoration of viability in the Api-HANP groups was equivalent to the protection provided by the Vitamin C positive control, which sustained. The cytoprotective effects of the nanocomposite were most significant at a dosage of 50 µM Api-HANPs (85%). Treatment with 100 µM Api-HANPs led to a significant reduction in viability relative to the 50 µM group. This signifies a biphasic response in which the 'mid-range' dose of 50 µM yields the greatest therapeutic advantage, while elevated doses may provoke secondary cellular stress due to increased nanoparticle density. Figure 5b illustrates that the MTT quantitative data

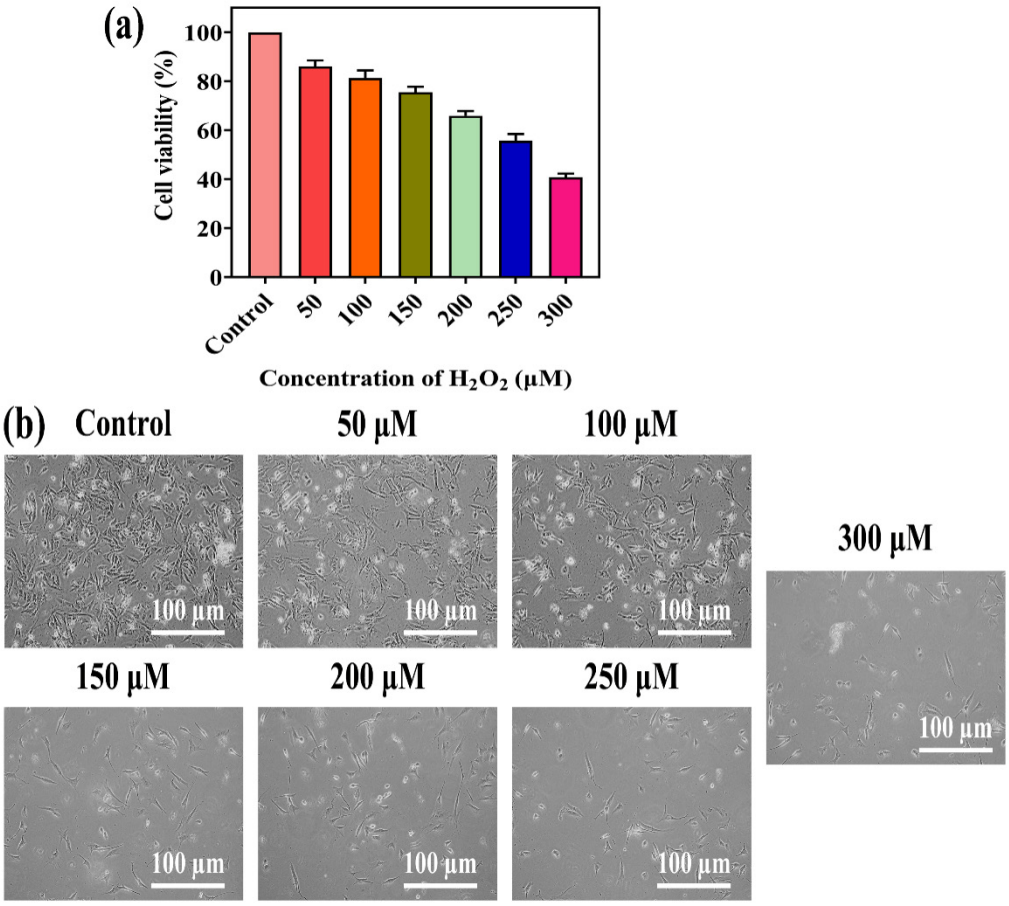

Figure 2: (a) Cytotoxicity and Cytoprotective Evaluation in H9c2 Cells. (a) Dose-dependent cytotoxicity of H_2O_2 (0-500 µM) on H9c2 cardiomyoblasts measured via MTT assay after 24 hr exposure. (b) Dose-response assessment of Api-HANP nanocomposites (5-100 µM) demonstrating the biocompatibility of the scaffold.

was corroborated by phase-contrast microscopy, revealing that Api-HANP (50 µM) and H_2O_2+Vit C pretreated cells exhibited a healthy spindle-shaped morphology and increased cell density, in contrast to the shrunken, apoptotic appearance observed in the H_2O_2 injury group. According to these findings, 50 µM was determined to be the best concentration for the Api-HANP nanocomposite to protect cardiomyoblasts from oxidative stress.

Effect of Api-HANPson apoptotic induction potential by AO/EtBr staining

In order to evaluate the ability of Api-HANPs and H_2O_2 to induce apoptosis, H_2O_2+Vit C, H9c2 cells were subjected to different doses of Api-HANPs and then exposed to H_2O_2 (Figure 6a, b). Afterwards, the cells were stained with AO/EtBr in order to observe apoptotic and necrotic morphological alterations. Pretreatment with Vitamin C (100 µM) markedly reduced H2O2-induced apoptosis, as indicated by a predominant population of green-fluorescing cells exhibiting intact nuclear architecture, akin to the control group. The positive control group effectively inhibited the transition to orange-red fluorescence, confirming that systematic antioxidant therapy preserves membrane integrity and prevents late-stage apoptotic alterations induced by oxidative damage. The AO/EtBr staining approach facilitated the identification of early and late apoptotic cells by observing their distinctive nuclear morphology. Early apoptotic cells had an orange-colored nucleus with compressed or fragmented chromatin, while late apoptotic cells exhibited a red nucleus with shattered and condensed chromatin. The

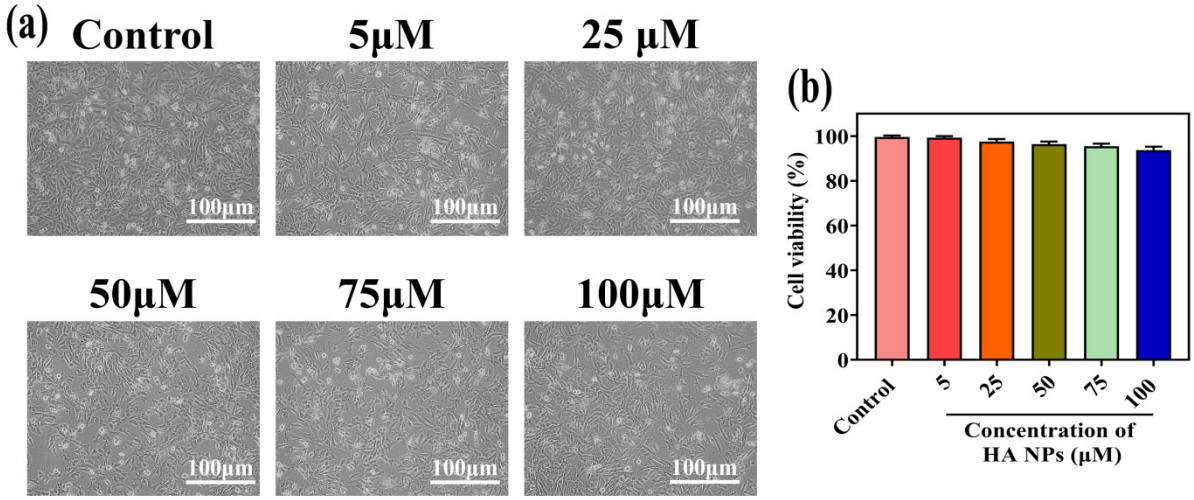

Figure 3: (a) Cytotoxicity and Cytoprotective Evaluation in H9c2 Cells. (a) Dose-dependent cytotoxicity of HANPs (5 – 100 µM) on H9c2 cardiomyoblasts measured via MTT assay after 24 hr exposure. (b) Dose-response assessment of HANP nanoparticles (5-100 µM) demonstrating the biocompatibility of the scaffold.

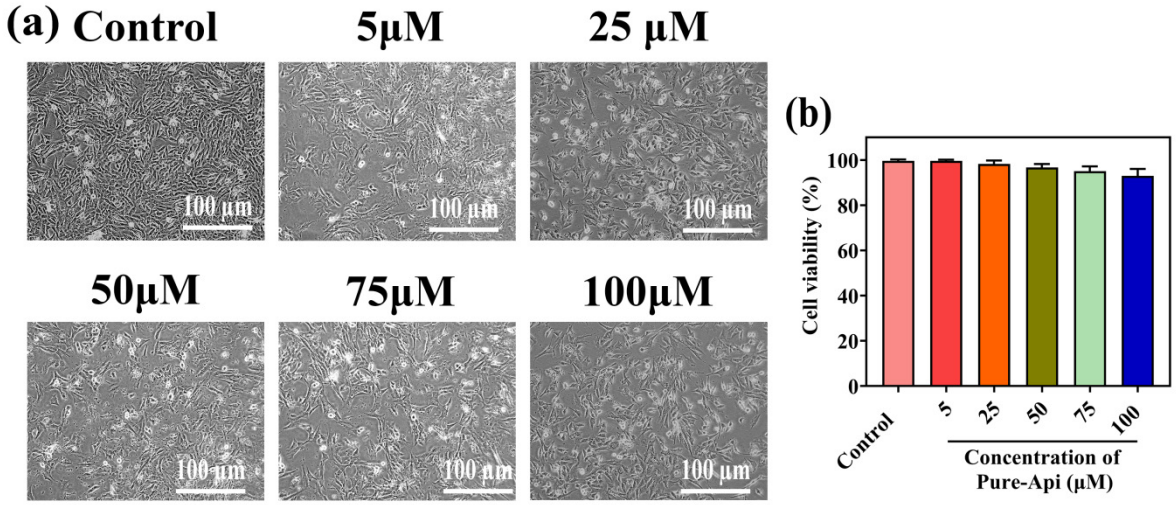

Figure 4: (a) Cytotoxicity and Cytoprotective Evaluation in H9c2 Cells. (a) Dose-dependent cytotoxicity of Pure Apigenin (5 – 100 µM) on H9c2 cardiomyoblasts measured via MTT assay after 24 hr exposure. (b) Dose-response assessment of Pure Apigenin (5-100 µM) demonstrating the biocompatibility of the scaffold.

findings of our study clearly showed that exposure to H_2O_2 alone triggered apoptosis in H9c2 cells, as shown by the presence of cells with orange and red nuclei. Nevertheless, prior treatment with Api-HANPs significantly decreased the quantity of cells undergoing apoptosis, especially at elevated doses. This indicates that Api-HANPs may have a protective impact against cell death in H9c2 cells when they are subjected to oxidative stress.

Impact of H_2O_2 and Api-HANPs on Antioxidant Enzyme Activity

SOD and Catalase (CAT) are antioxidant enzymes that have a crucial function in safeguarding the heart from the harmful impact of ROS. Imbalance in the functioning of these enzymes is often associated with the underlying causes of CVD. The outcomes of our investigation revealed a substantial reduction in the activity of SOD and CAT in cells treated with H_2O_2 in comparison to the control cells ($p < 0.0001$), H_2O_2+Vit C, H_2O_2-Api-HANPs (Figure 7 a, b). This suggests that the presence of H_2O_2 might cause oxidative stress, which in turn can decrease the cells' ability to defend against antioxidants. In contrast, prior treatment with Api-HANPs led to a significant elevation in SOD and CAT activity when compared to cells treated to H_2O_2 ($p < 0.0001$). These findings indicate that Api-HANPs may enhance the cells' antioxidant defense systems, hence contributing to their cytoprotective benefits.

Effect of Api-HANPs on Lipid Peroxidation

The enzymatic decomposition of lipids by ROS is known as lipid peroxidation. Damage and disturbance to cells might be possible outcomes. This study evaluated MDA levels as a measure of lipid peroxidation. In our investigation, H_2O_2-treated cells exhibited significantly higher levels of MDA compared to control cells ($p < 0.0001$), confirming that oxidative stress induces lipid peroxidation (Figure 7c). Importantly, compared to cells exposed to H_2O_2, those pre-treated with Api-HANPs showed a significant decrease in MDA levels ($p < 0.0001$). These findings suggest that

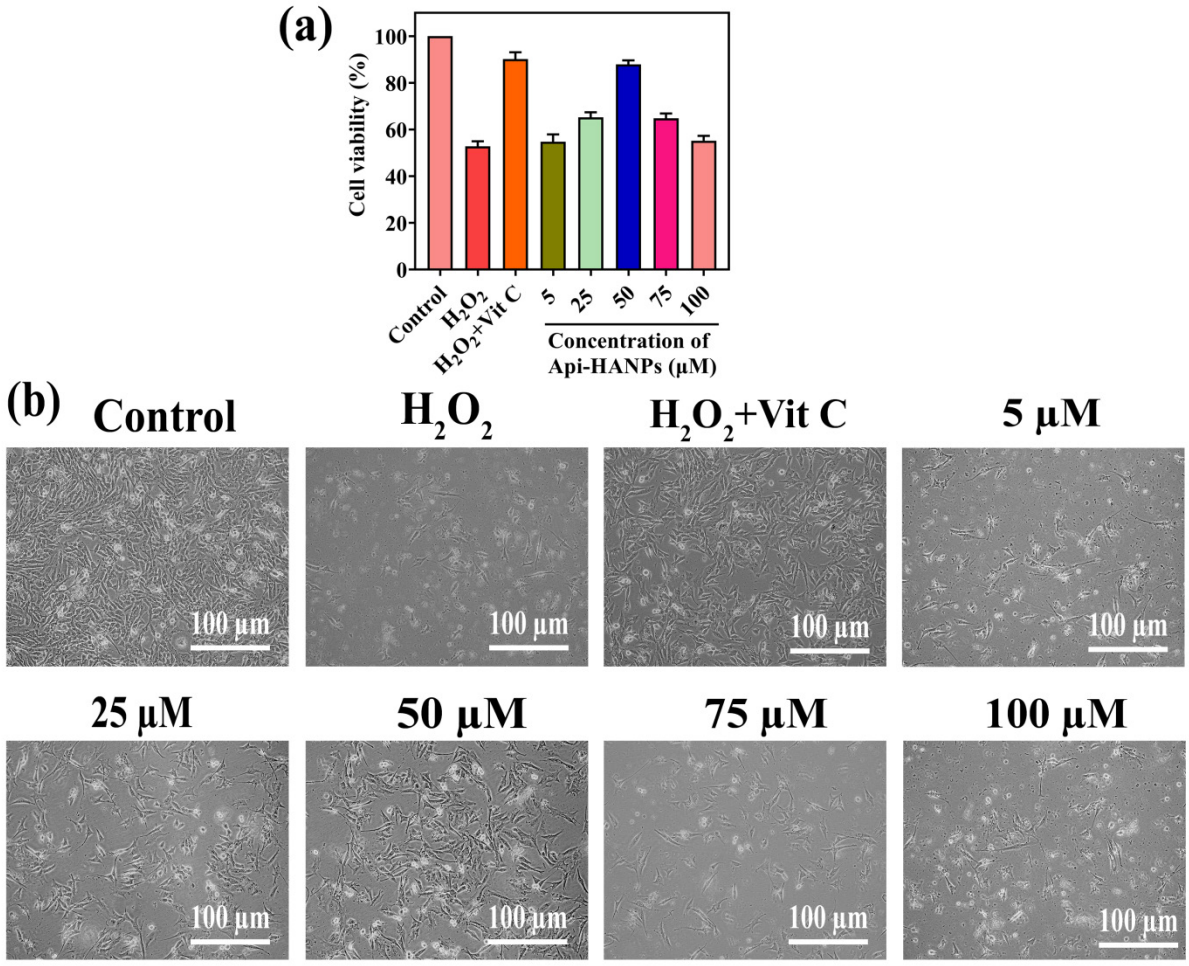

Figure 5: Api-HANPs' cytoprotective effect on H9c2 cardiomyoblasts induced injury by H2O2. (a) Api-HANPs' defense against H2O2-induced loss of cell viability. The cells were treated with 250 µM of H2O2 for 1 hr, after being pretreated with diverse concentrations of Api-HANPs (5-100 µM) for one day. (b) Microscopy images of H2O2 (250 µM), H2O2+ VitC (100 M) and different concentrations of Api-HANPs (5, 25, 50, 75, and 100 µM) for one day and H2O2 (250 µM) treatment for 1 hr. The three separate experiments' mean ± SD are included in the data. In comparison to the control, *#p < 0.0001. In comparison to the H2O2-treated group, *p < 0.0001.

Api-HANPs effectively inhibit lipid peroxidation and protect cellular components from oxidative stress.

Effect of Api-HANPs on intercellular ROS generation by DCFH DA

The DCFH-DA fluorescent probe was employed to evaluate the impact of H_2O_2-Api-HANPs on intracellular ROS generation (Figure 8a, b). Our findings demonstrated a considerable increase in green fluorescence intensity in cells subjected to H_2O_2 (250 μM) relative to the control group, indicating a significant rise in ROS production. This result corresponds with the recognized pro-oxidant properties of H_2O_2 in cardiomyoblast models. In contrast, pretreatment with either Api-HANPs or the positive control, H_2O_2+Vit C led to a marked reduction in fluorescence intensity compared to the H_2O_2 challenged group ($p < 0.001$). The ROS-scavenging ability of 50 μM Api-HANPs was remarkably effective, achieving a decrease in oxidative species similar to that of the Vitamin C standard. These findings indicate that Api-HANPs

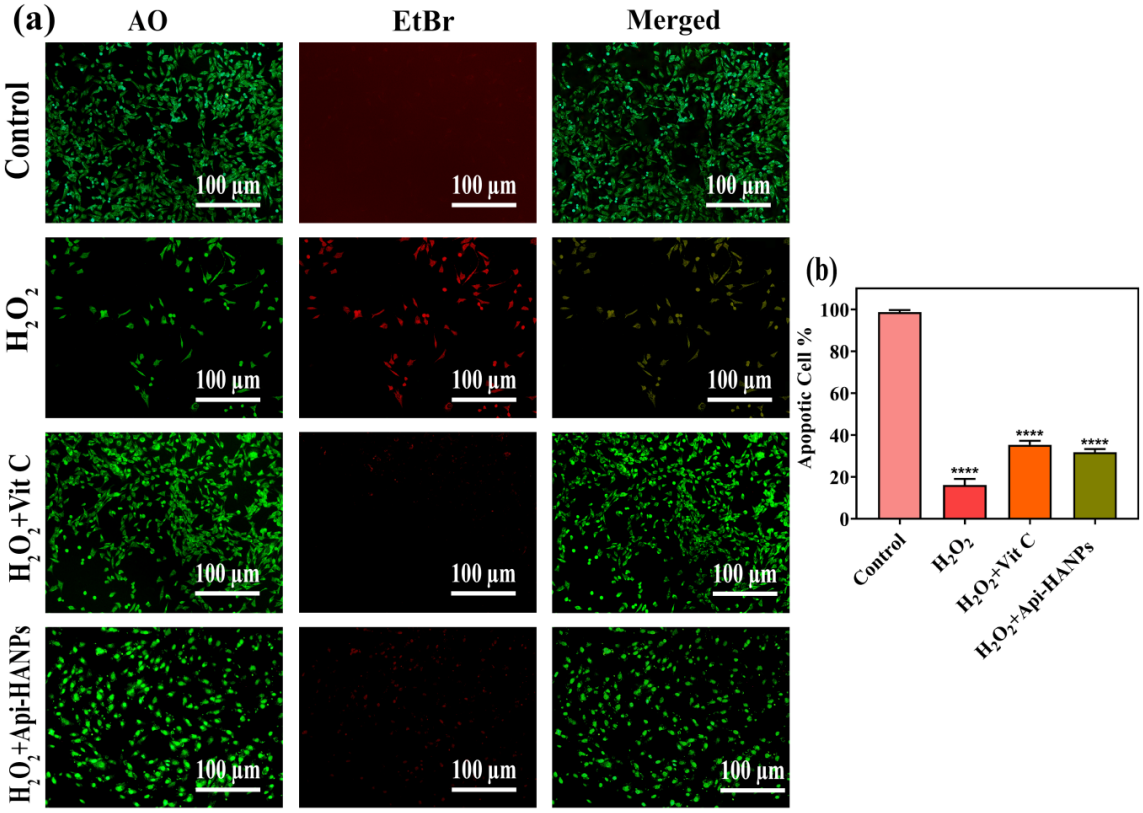

Figure 6: Apoptotic alterations caused by Api-HANPs were examined using AO/EtBr staining. (a) Fluorescence microscopic analysis of control, H2O2 (250 μM), H2O2+ Vit C (100 μM) and Api-HANPs+H2O2 (50 μM) cells. (b) Bar diagram shows apoptotic cell percentage. Data from three separate trials are presented as mean ± SD. ## p< 0.0001 vs. control, ** vs. H2O2 groups.

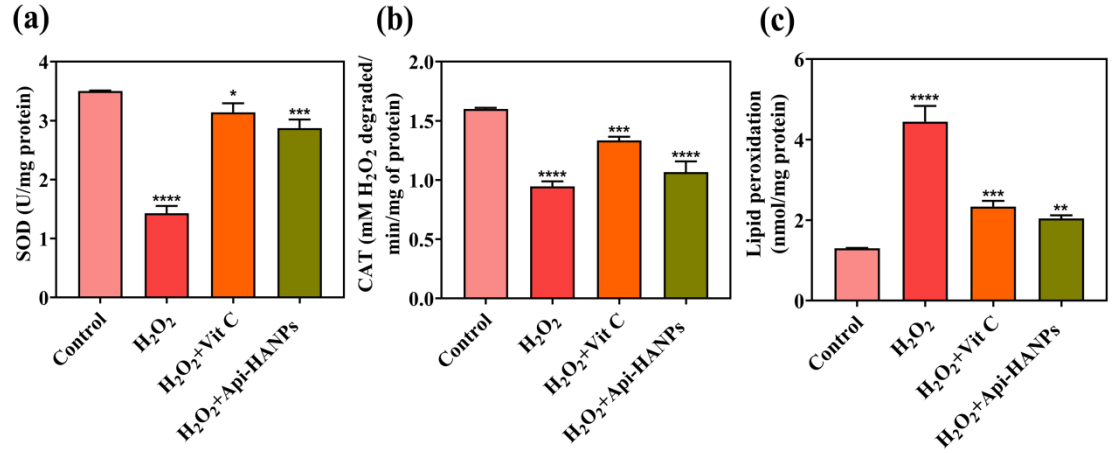

Figure 7: (a-c) The protective effect of Api-HANPs against H2O2 damage in an antioxidant enzyme test using SOD, Catalase, and lipid peroxidation. The data are shown as the mean ± standard deviation from 3 separate trials. ##p< 0.0001 compared to the control group. As compared to the H2O2-treated groups, **p< 0.0001.

protect H9c2 cells by effectively reducing ROS production and preserving intracellular redox equilibrium. The quantitative fluorescence results (Figure 8b) further substantiates that the integrated nanocomposite functions as an effective antioxidant reservoir, offering a protective barrier against peroxide-induced oxidative damage.

Effect of Api-HANPs on Mitochondrial Membrane Potential (MMP)

Mitochondrial Membrane Potential (MMP) is a crucial factor in maintaining mitochondrial homeostasis and cellular survival; a prolonged decrease in MMP results in cellular dysfunction and the activation of apoptotic pathways. We employed the lipophilic cationic dye Rh-123 (Figure 9a, b) to assess the protective effect of Api-HANPs on mitochondrial integrity. Our analysis revealed a substantial decrease in Rh-123 fluorescence intensity in cells subjected to H_2O_2 (250 µM) compared to the control group, suggesting that H_2O_2 induced oxidative stress results in the depolarization of the inner mitochondrial membrane. Conversely, pretreatment with either Api-HANPs or the positive control, H_2O_2+Vit C led to a considerable maintenance of MMP levels in comparison to the H_2O_2 treated cells ($p < 0.01$). The Vitamin C group exhibited a significant cytoprotective impact, reinstating mitochondrial polarization and preserving Rh-123 retention. The 50 µM Api-HANP group had a similar capacity to stabilize the mitochondrial membrane potential. The findings indicate that Api-HANPs protect H9c2 cells by maintaining mitochondrial structural integrity and averting metabolic failure linked to oxidative stress. Figure 9b quantitative study substantiates that the nanocomposite efficiently alleviates mitochondrial dysfunction, a critical factor in averting cardiomyoblast apoptosis.

Effect of Api-HANPs on nuclear staining using DAPI

DAPI fluorescence labeling was utilized to assess the effects of Api-HANPs on nuclear architecture and nucleus integrity (Figure 10). Our findings indicated notable morphological defects typical of late-stage apoptosis in cells subjected to H_2O_2 (250 µM). The modifications encompassed pronounced nuclear contraction (pyknosis), chromatin condensation, and the emergence of apoptotic structures, all indicative of permanent chromosomes damage and programmed cell death. Conversely, cells pretreated with either H_2O_2-Api-HANPS (50 µM) and the positive control, H_2O_2+Vit C, had a well-maintained nuclear architecture. The group treated with Vitamin C exhibited a notable decrease in apoptotic characteristics, preserving consistent nuclear size and intact chromatin distribution akin to the control group. Likewise, H_2O_2-Api-HANP pretreatment successfully inhibited the nuclear fragmentation and shrinkage linked to H_2O_2 toxicity. The results indicate that Api-HANPs protect H9c2 cells by preserving nuclear integrity and inhibiting the DNA fragmentation that usually

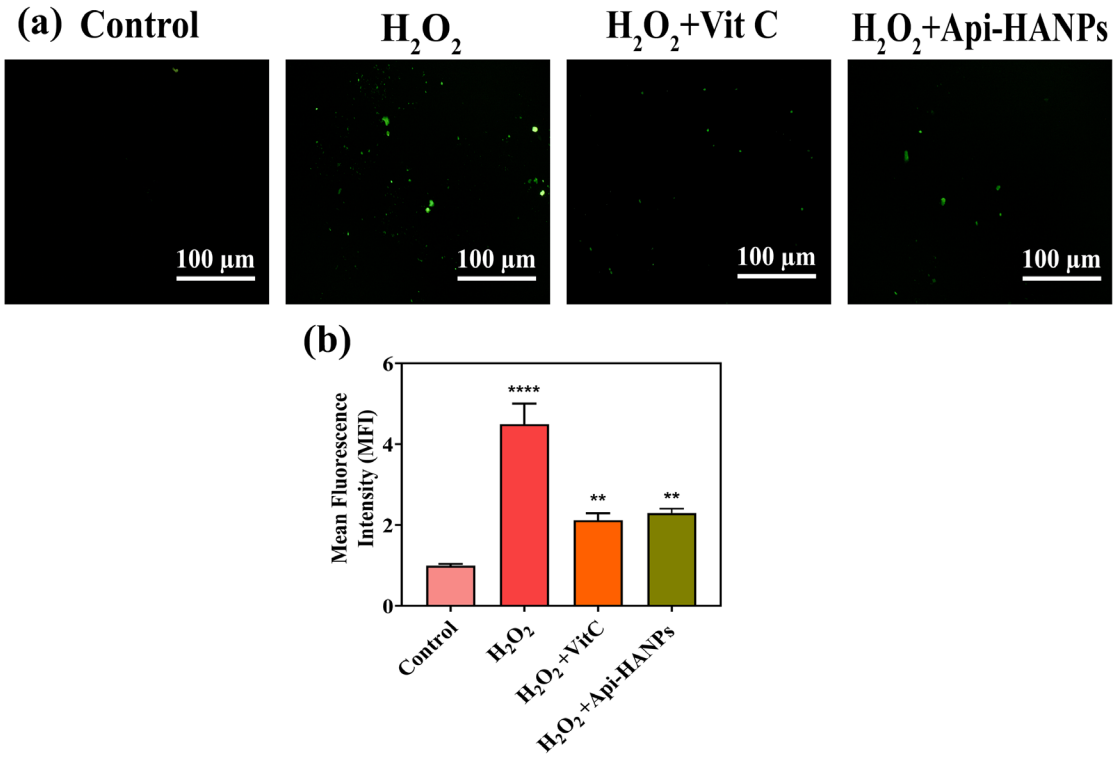

Figure 8: (a) Micrographs of ROS production caused by DCFH-DA staining control, H2O2 (250 µM), H2O2+ VitC (100 M) and Api-HANPs+ H2O2 (50 µM); (b) Image J software was used to measure the strength of DCFH-mediated fluorescence, which showed the amount of ROS inside the cells. The numbers are given as the average light level (±SD) of five fields of view in each group. The data are shown as the mean ± standard deviation from three separate trials. **p< 0.0001 compared to the control group. ##p< 0.0001 compared to the H2O2 treatment group.

occurs after oxidative-stress-induced mitochondrial failure. Figure 10's qualitative observations validate that the Api-HANP system offers a strong protective barrier for the genetic material of cardiomyoblasts.

Molecular Docking Analysis of Apigenin-NF-κB Interaction

Molecular docking studies utilizing AutoDock demonstrated that apigenin exhibits stable binding into the active region of the NF-κB protein, located at grid coordinates X = 0.0540, Y = 71.789, Z = 80.507, with a favorable binding affinity of −7.7 kcal/mol. The highest-ranked posture exhibited exceptional convergence, with RMSD lower and upper bounds of 0.000 Å, hence affirming stable orientation. Apigenin was predominantly stabilized by hydrophobic and van der Waals contacts with residues ILE354 and PRO352, forming a nonpolar pocket with favorable shape complementarity, despite a scarcity of hydrogen bonds and interacting residues (Figure 11a, b and Table 1). The energetically favorable binding corroborates apigenin's putative interaction with NF-κB, providing computational validation that enhances the results of experiments.

Api-HANPs regulated NF-kB and Nrf2 expression in H9C2 cells under H_2O_2 condition

Immunofluorescence labelling was conducted to assess the modulation of nuclear translocation of essential transcription factors by Api-HANPs during H2O2-induced stress. Figure 12a demonstrates that H_2O_2 therapy significantly increased the nuclear translocation of the inflammatory factor NF-κB p65, as indicated by pronounced localized staining within the nucleus relative to the control group. This verifies that H_2O_2 induces a strong inflammatory response in H9c2 cells. In contrast, pretreatment with either Api-HANPs or the positive control, H_2O_2+Vit C, effectively mitigated this translocation, predominantly maintaining NF-κB p65 in the cytoplasm and reinstating nuclear localization to levels comparable to the control. This illustrates the significant anti-inflammatory capability of the nanocomposite. Moreover, exposure to H_2O_2 led to a reduction

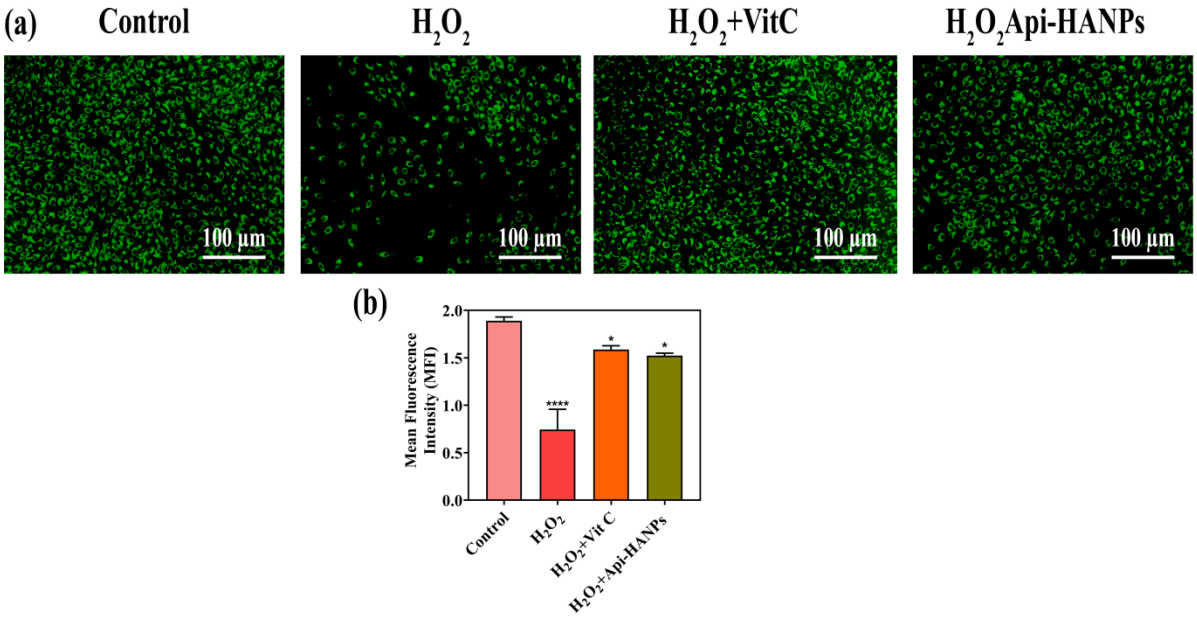

Figure 9: (a) Microscopic pictures of MMP assessed using Rh-123 staining: control, H_2O_2 treated, H_2O_2+VitC, and Api-HANPs+H_2O_2; (b) The intensity of Rh-123-mediated fluorescence was measured utilizing Image J software. ##$p < 0.0001$ compared to control. **$p < 0.0001$ compared to H_2O_2 treated groups.

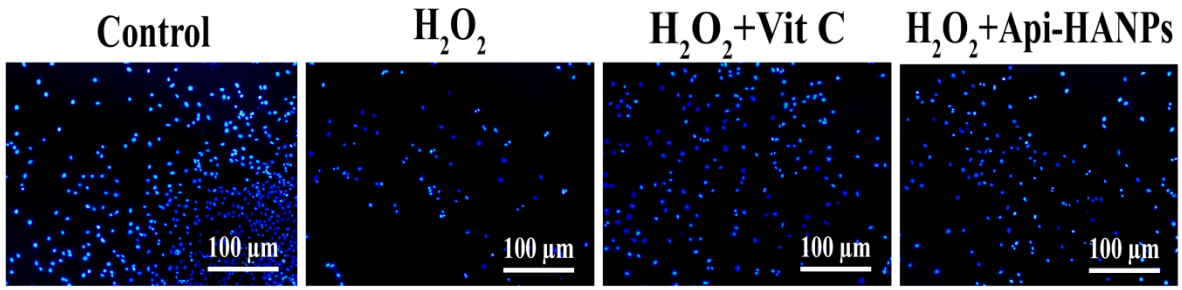

Figure 10: DAPI staining experiment of control, H_2O_2-treated, H_2O_2+VitC, and Api-HANPs+H_2O_2 showing apoptotic cells exhibiting blurred membranes and apoptotic bodies.

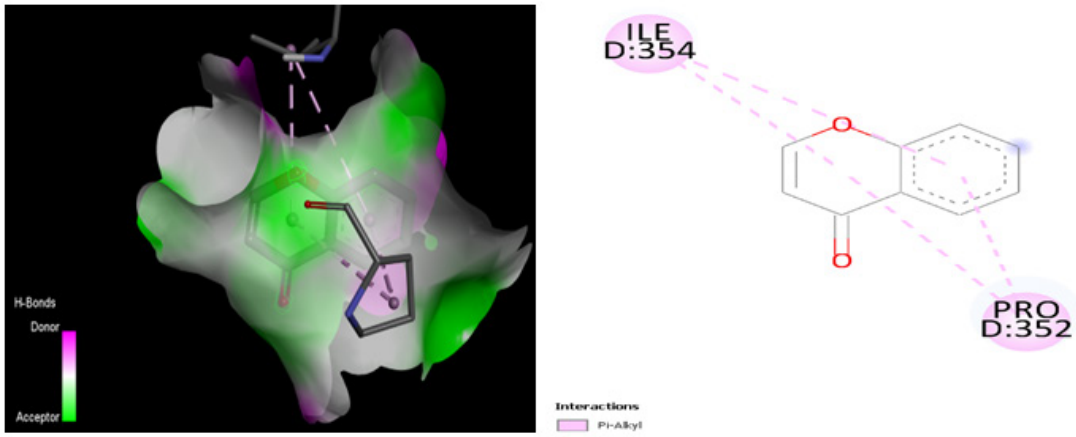

Figure 11: 3D and 2D Interaction for Apigenin and NF-κB.

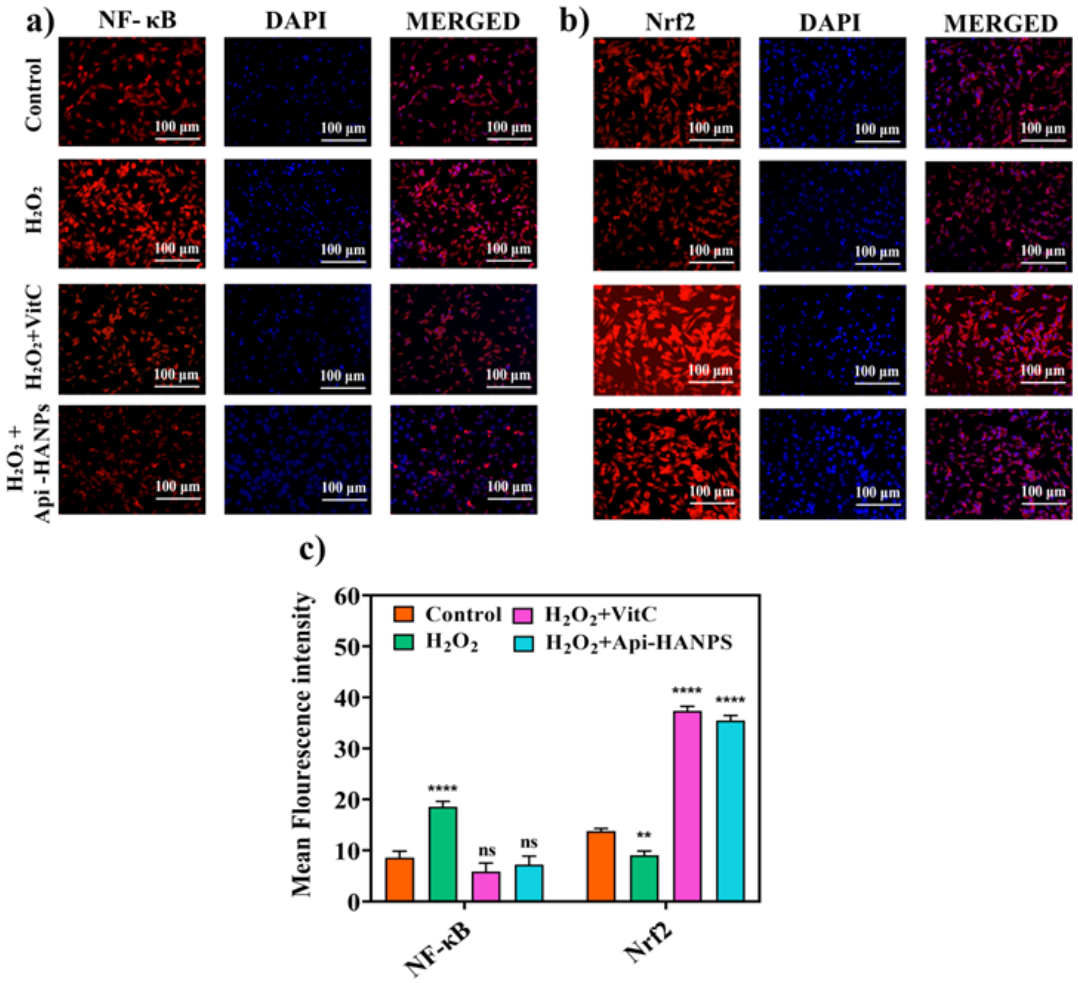

Figure 12: NF-kB immunofluorescence staining of control, H_2O_2 treated, H_2O_2+VitC, and Api-HANPs+H_2O_2; (b) Mean Nrf2 immunofluorescence staining of control, H_2O_2 treated, H_2O_2+VitC, and Api-HANPs+H_2O_2.

in nuclear expression of the antioxidant transcription factor Nrf2, indicating that intense oxidative stress compromises the cell's inherent defense mechanisms (Figure 12b). Pretreatment with Vitamin C acted as a protective standard, aiding in the preservation of Nrf2 levels. Api-HANP administration markedly enhanced the nuclear accumulation of Nrf2, likely improving the downstream antioxidant response more efficiently than the free antioxidant. The twin outcomes demonstrate that Api-HANPs offer an advanced defense mechanism against H_2O_2 induced damage by concurrently inhibiting the pro-inflammatory NF-κB pathway and activating the cytoprotective Nrf2 pathway, thus efficiently reinstating cellular homeostasis.

Table 1: The binding affinities (in kcal/mol) and structural deviations (RMSD) of various apigenin isomers to the NFκB protein. The lower bound (rmsdl.b.) and upper bound (rmsdu.b.) represent the minimum and maximum RMSD values, respectively, for each binding mode. A lower RMSD indicates a more similar conformation to the optimal binding mode.

Name	Binding Affinity (kcal/mol)	Distance from RMSD [LB]	Distance from RMSD [UB]	Protein Co-ordinate Values
Apigenin	-7.7	0.000	0.000	X - 0.0540 Y - 71.789 Z - 80.507

DISCUSSION

The enhanced cardioprotective efficacy of the Api-HANP system demonstrated in this study is most comprehensively appreciated in relation to existing literature. Previous studies on the cardioprotective properties of apigenin have primarily concentrated on its capacity to modulate cardiac microRNAs and alleviate isoproterenol-induced damage.[40,41] Although these trials demonstrate apigenin as an effective nutraceutical, they depend on elevated systemic dosages of the unbound molecule, which is limited by inadequate bioavailability. Recent studies have employed silver and gold nanoparticles (AgNPs/AuNPs) in nanoparticle-based antioxidant systems to assess antioxidant capacity and to deliver apigenin for the mitigation of doxorubicin-induced cardiotoxicity.[42,43] Although efficient, metallic nanoparticles may raise challenges related to long-term biosafety and the potential development of secondary oxidative stress in vulnerable cardiac tissues. Our research presents an innovative framework by employing HANP a biomimetic mineral. In contrast to AgNPs or AuNPs, HANPs provide a naturally inert and solvent-free framework that emulates the endogenous calcium phosphate found in biological systems. This guarantees that the detected activation of the Nrf2/NF-κB pathway is solely a reaction to the stable apigenin 'reservoir' rather than an interaction with an external metallic carrier, thereby broadening the use of HANPs from bone engineering to soft-tissue cardioprotection.

A novel Api-HANPs nanocomposite was produced and evaluated for cytoprotection on oxidatively challenged H9c2 cardiomyoblasts. Apigenin inclusion on HANPs and the nanocomposite minimize H_2O_2-induced cellular damage via synergistic processes. Api-HANPs nanocomposite synthesis was verified by FTIR, XRD, and FESEM. FTIR verified apigenin-HANPs molecular interaction. HANPs phosphate peaks changing suggest hydrogen bonding or electrostatic interactions, with Apigenin C=O peak shifting. These interactions are essential for composite stability and drug loading. XRD showed apigenin inclusion in the Api-HANPs nanocomposite showed weaker crystalline peaks compared to pure HANPs. Apigenin amorphous nature and interaction with the HANPs lattice disrupt its long-range ordering, lowering crystallinity. Structural alterations that enhance surface area and reduce crystal size may improve drug loading and release rates in drug delivery devices.

Morphological alterations were seen in FESEM. More heterogeneous than pure HANPs, the Api-HANPs nanocomposite was rod-like and spherical. Apigenin altered HANP self-assembly and crystallization, generating a complex surface topography with increased roughness. For prolonged therapeutic benefits in cardiac tissue engineering, drug delivery applications need expanded surface area and numerous binding sites to optimize drug-carrier interactions and controlled release. In our study cytoprotective was observed in 50 μM (Figure 2a, b). Previous study reported that pretreatment with different concentrations of apigenin reduced cytotoxicity in ISO-treated H9c2 cells.[44] The apoptosis of H9c2 cells was evaluated by AO/EtBr staining. The Api-HANPs treated cells showed significantly decreased compared to H_2O_2 exposed cells. The current study agrees well with the study.[45] The Api-HANPs-pretreated cells exhibit antioxidant assay levels of SOD and CAT followed by exposed to H_2O_2 (Figure 5a, b). The elevated level of SOD and CAT can be attributed to the proliferative activity of Api-HANPs in H9c2 rat cardiomyocytes. These results are supported by research that shows apigenin increases the expression of important antioxidant enzymes like glutathione synthase, catalase, and superoxide dismutase, thereby boosting the cellular antioxidant defense mechanism. Furthermore, by inhibiting NADPH oxidase activity and thus downregulating related pro-inflammatory genes, apigenin demonstrates anti-inflammatory properties.[46] Oxidative stress leads to the release of malondialdehyde, a result of the oxidation of lipid bilayers and other lipid molecules. In our investigation, the pretreatment of Api-HANPs resulted in a decrease in MDA levels, while cells treated with H_2O_2 alone showed an increase in MDA levels (Figure 5c). The reduced levels of MDA content may be attributed to the increased amounts of intracellular antioxidants in cardiomyocytes. Thus, it was demonstrated that pretreatment with Api-HANPs reduced the oxidation of lipid bilayer and other lipid components. Our result is consistent with the report of.[47]

The microscopic examinations revealed evident alterations in the cellular structure, including decreased cell size, the formation of blebs, and cell shrinkage, which are indicative of apoptosis in cells treated with H_2O_2. Cells that were pretreated with Api-HANPs

exhibited a significantly reversal of cell damage. Typically, cells that undergo apoptosis will display cellular damage characterized by irregular cell morphologies, cell shrinkage, blebbing, DNA damage, and chromatin condensation.[48] The use of DCFDA labeling revealed a strong green fluorescence in cells exposed to H_2O_2, indicating the presence of ROS. In contrast, cells pretreated with Api-HANPs showed absence of fluorescence, compared to the control cells which was concordant with the previous report.[49]

An early stage of cellular death, the mitochondrial permeability transition pore, can be activated by oxidative stress. A crucial component for sustaining cellular energy production, the mitochondrial membrane potential (ΔΨm), is lost during this process. Overexposure to oxidants can cause damage to the mitochondria, which can then compromise mitochondrial function and ultimately cause cellular malfunction.[50] Cells treated with Api-HANPs followed by exposed to H_2O_2 cells showed significantly prevented the loss of mitochondrial membrane potential (ΔΨm), as shown in Figure 7. A previous study has documented that protective effect of apigenin in mitochondrial function in osteoblastic cells.[51] The current results demonstrate a beneficial interaction between apigenin and the NF-κB pathway protein, demonstrated by a binding energy of −7.7 kcal/mol, indicating a thermodynamically stable ligand-protein connection. This association is additionally reinforced by the participation of critical hydrophobic residues, ILE(D):354 and PRO(D):352, which enhance complex stability inside a nonpolar binding pocket. The results indicate that apigenin may successfully bind to the NF-κB protein, offering computational support for its putative function in altering NF-κB-related signaling. These results align with previous studies highlighting the anti-inflammatory properties of Apigenin.Immunostaining findings validated the computational analysis, demonstrating that Api-HANPs administration effectively suppressed the H_2O_2-induced nuclear translocation of the inflammatory transcription factor NF-κB p65, thereby reducing the inflammatory cascade.[52] Simultaneously, Api-HANPs promoted the nuclear translocation of the antioxidant transcription factor Nrf2, essential for initiating the cellular antioxidant response.[53]

CONCLUSION

This work successfully fabricated a new Api-HANPs nanocomposite and offers strong evidence of its considerable cytoprotective properties against H_2O_2-induced oxidative stress in H9c2 cardiomyoblasts. The physicochemical investigations validate the successful integration of apigenin with HANPs, which modifies the material's characteristics beneficially for biological applications. The biological findings indicate that Api-HANPs not only alleviate significant indicators of oxidative damage, such as diminished cell viability, heightened apoptosis, and increased lipid peroxidation, but also reinstate essential cellular functions by augmenting antioxidant enzyme activity, safeguarding mitochondrial integrity, and preserving nuclear structure. The therapeutic potential of the nanocomposite is clarified by its dual-modulatory action on essential cellular pathways: it inhibits the inflammatory NF-κB pathway while concurrently stimulating the antioxidant Nrf2 pathway. Notwithstanding these encouraging outcomes, a few limitations must be recognized. Initially, the *in vitro* design of this work and the use of the H9c2 cardiomyoblast line, which embodies a neonatal-like phenotype, may not entirely reflect the physiological intricacies of adult cardiomyocytes. Secondly, although our molecular docking and biochemical assays offer mechanistic insights, additional investigations employing Western blotting and RT-PCR are necessary in order to better quantify protein expression and gene transcription levels. The lack of long-term toxicity evaluations and in vivo validation continues to provide a difficulty for clinical translation. Subsequent investigations need to concentrate on animal models to evaluate systemic biocompatibility, pharmacokinetics, and true therapeutic efficacy in a real cardiac system. Nonetheless, the present findings suggest that the Api-HANP nanocomposite holds considerable promise as a therapeutic agent for protecting heart tissue from oxidative injury.

ACKNOWLEDGEMENT

None.

ABBREVIATIONS

ACE: Angiotensin-Converting Enzyme; **ANOVA:** Analysis of Variance; **AO/EB:** Acridine Orange/Ethidium Bromide; **Api-HANPs:** Apigenin-Hydroxyapatite Nanocomposite; **CAT:** Catalase; **CID:** Compound Identifier; **CVD:** Cardiovascular Disease; **DAPI:** 4′,6-Diamidino-2-Phenylindole; **DCFH-DA:** 2′,7′-Dichlorofluorescin Diacetate; **DD water:** Double Distilled Water; **DMEM:** Dulbecco's Modified Eagle's Medium; **FBS:** Fetal Bovine Serum; **FESEM:** Field Emission Scanning Electron Microscopy; **FTIR:** Fourier Transform Infrared Spectroscopy; **H_2O_2:** Hydrogen Peroxide; **HANPs:** Hydroxyapatite Nanoparticles; **I/R:** Ischemia/Reperfusion; **MDA:** Malondialdehyde; **MFI:** Mean Fluorescence Intensity; **MI:** Myocardial Infarction; **MMP:** Mitochondrial Membrane Potential; **MTT:** 3-(4,5-Dimethylthiazol-2-yl)-2,5-Diphenyltetrazolium Bromide; **NF-κB:** Nuclear Factor Kappa B; **Nrf2:** Nuclear Factor Erythroid 2-Related Factor 2; **PBS:** Phosphate-Buffered Saline; **Rh-123:** Rhodamine 123; **RT:** Room Temperature; **ROS:** Reactive Oxygen Species; **SD:** Standard Deviation; **SOD:** Superoxide Dismutase; **SS:** Stainless Steel; **TBARS:** Thiobarbituric Acid Reactive Substances; **XRD:** X-ray Diffraction; **ΔΨm:** Mitochondrial Membrane Potential (Delta Psi m).

CONFLICT OF INTEREST

The authors declare that there is no conflict of interest.

SUMMARY

This study developed an Api-HANPs to enhance apigenin's cardioprotective potential against oxidative stress. The nanocomposite was synthesized and characterized using FTIR, XRD, and FESEM. In H9c2 cardiomyoblasts exposed to H_2O_2, Api-HANPs significantly improved cell viability, reduced apoptosis, lipid peroxidation, and ROS generation, while restoring antioxidant enzymes (SOD, CAT) and mitochondrial function. Molecular docking showed strong binding of apigenin to NF-κB (-7.7 kcal/mol), and immunostaining revealed activation of Nrf2 and inhibition of NF-κB. Overall, Api-HANPs effectively mitigated oxidative and inflammatory injury, indicating their promise as a nanotherapeutic agent for cardiovascular protection.

REFERENCES

1. Abdunabieva K. Cardiovascular diseases (EG, HYPERTENSION, HEART ATTACK). Int J Med Sci. 2025;1(3):20-4. doi: 10.55640.
2. Mansour RM, Hemdan M, Moustafa HA, Mageed SS, Rizk NI, Ali MA, *et al*. Global Perspectives on Coronary Artery Disease: The Emerging Role of miRNAs. CurrAtheroscler Rep. 2025;27(1):66. doi.org/10.1007/s11883-025-01309-8.
3. Sulashvili N, Nimangre RR. Manifestation of some aspects of cardiovascular diseases, implications, pharmacotherapeutic strategies, effects, impacts and potential hazards in general. Junior Res. 2025;3(1):1-27. doi: 10.52340/jr.2025.03.01.01.
4. Ramos-Regalado L, Alcover S, Badimon L, Vilahur G. The influence of metabolic risk factors on the inflammatory response triggered by myocardial infarction: bridging pathophysiology to treatment. Cells. 2024;13(13):1125. doi: 10.3390/cells13131125.
5. Zhang S, Yang Y, Lv X, Liu W, Zhu S, Wang Y, *et al*. Unraveling the intricate roles of exosomes in cardiovascular diseases: A comprehensive review of physiological significance and pathological implications. Int J Mol Sci. 2023;24(21):15677. doi: 10.3390/ijms242115677.
6. He J, Liu D, Zhao L, Zhou D, Rong J, Zhang L, *et al*. Myocardial ischemia/reperfusion injury: Mechanisms of injury and implications for management. Exp Ther Med. 2022;23(6):430. doi: 10.3892/etm.2022.11357.
7. Liu J, Han X, Zhang T, Tian K, Li Z, Luo F. Reactive oxygen species (ROS) scavenging biomaterials for anti-inflammatory diseases: from mechanism to therapy. J HematolOncol. 2023;16(1):116. doi: 10.1186/s13045-023-01512-7.
8. Woo SH, Kim JC, Eslenur N, Trinh TN, Do LN. Modulations of cardiac functions and pathogenesis by reactive oxygen species and natural antioxidants. Antioxidants. 2021;10(5):760. doi: 10.3390/antiox10050760.
9. Hussain G, Zhang L, Rasul A, Anwar H, Sohail MU, Razzaq A, *et al*. Role of plant-derived flavonoids and their mechanism in attenuation of Alzheimer's and Parkinson's diseases: An update of recent data. Molecules. 2018;23(4):814. doi: 10.3390/molecules23040814.
10. Yunusoğlu O, Ayaz İ, Dovankaya EH. Pharmacological, medicinal and biological properties of flavonoids: A comprehensive review. J Res Pharm. 2025;29(2):561-84. doi: 10.12991/jrespharm.1661054.
11. Melrose J. The potential of flavonoids and flavonoid metabolites in the treatment of neurodegenerative pathology in disorders of cognitive decline. Antioxidants. 2023;12(3):663. doi: 10.3390/antiox12030663.
12. Hassan SS, Samanta S, Dash R, Karpiński TM, Habibi E, Sadiq A, *et al*. The neuroprotective effects of fisetin, a natural flavonoid in neurodegenerative diseases: Focus on the role of oxidative stress. Front Pharm. 2022;13:1015835. doi: 10.3389/fphar.2022.1015835.
13. Singh A, Singh J, Parween G, Khator R, Monga V. A comprehensive review of apigenin a dietary flavonoid: biological sources, nutraceutical prospects, chemistry and pharmacological insights and health benefits. Crit Rev Food SciNutr. 2025;65(23):4529-65. doi: 10.1080/10408398.2024.2390550.
14. Abid R, Ghazanfar S, Farid A, Sulaman SM, Idrees M, Amen RA, *et al*. Pharmacological properties of 4 , 5, 7-trihydroxyflavone (apigenin) and its impact on cell signaling pathways. Molecules. 2022;27(13):4304. doi: 10.3390/molecules27134304.
15. Gao HL, Yu XJ, Hu HB, Yang QW, Liu KL, Chen YM, *et al*. Apigenin improves hypertension and cardiac hypertrophy through modulating NADPH oxidase-dependent ROS generation and cytokines in hypothalamic paraventricular nucleus. CardiovascToxicol. 2021;21(9):721-36. doi: 10.1007/s12012-021-09662-1.
16. Ginwala R, Bhavsar R, Chigbu DG, Jain P, Khan ZK. Potential role of flavonoids in treating chronic inflammatory diseases with a special focus on the anti-inflammatory activity of apigenin. Antioxidants. 2019;8(2):35. doi: 10.3390/antiox8020035.
17. Li Z, Zhou J, Ji L, Liang Y, Xie S. Recent advances in the pharmacological actions of apigenin, its complexes, and its derivatives. Food Rev Int. 2023;39(9):6568-601. doi: 10.1080/87559129.2022.2122989.
18. Allemailem KS, Almatroudi A, Alharbi HO, AlSuhaymi N, Alsugoor MH, Aldakheel FM, *et al*. Apigenin: a bioflavonoid with a promising role in disease prevention and treatment. Biomedicines. 2024;12(6):1353.doi: 10.3390/biomedicines12061353.
19. Salehi B, Venditti A, Sharifi-Rad M, Kręgiel D, Sharifi-Rad J, Durazzo A, *et al*. The therapeutic potential of apigenin. Int J Mol Sci. 2019;20(6):1305. doi: 10.3390/ijms20061305.
20. Kashyap P, Shikha D, Thakur M, Aneja A. Functionality of apigenin as a potent antioxidant with emphasis on bioavailability, metabolism, action mechanism and in vitro and in vivo studies: A review. J Food Biochem. 2022;46(4):e13950. doi: 10.1111/jfbc.13950.
21. Naeem A, Ming Y, Pengyi H, Jie KY, Yali L, Haiyan Z, *et al*. The fate of flavonoids after oral administration: A comprehensive overview of its bioavailability. Crit Rev Food SciNutr. 2022;62(22):6169-86. doi: 10.1080/10408398.2021.1898333.
22. Turon P, Del Valle LJ, Alemán C, Puiggalí J. Biodegradable and biocompatible systems based on hydroxyapatite nanoparticles. Appl Sci. 2017;7(1):60. doi: 10.3390/app7010060.
23. Hossain N, Chowdhury MS, Sarker MA, Huda MN, RajibHamam M, Islam S, *et al*. Synthesis Morphological and Antimicrobial Characterization of Hydroxyapatite Nanoparticles for Biomedical Applications. Nano. 2024;2450095. doi: 10.1142/S1793292024500954.
24. Thulasimuthu E, Veeramani S, Rajangam I. Effect of dual-doped hydroxyapatite nanoparticles loaded with 5-fluorouracil on breast cancer treatment through the disruption of DNA replication: *In vitro* drug release and kinetics study. BioNanoSci. 2025;15(1):130. doi: 10.1007/s12668-024-01644-1.
25. Montone AM, Papaianni M, Malvano F, Capuano F, Capparelli R, Albanese D. Lactoferrin, quercetin, and hydroxyapatite act synergistically against Pseudomonas fluorescens. Int J Mol Sci. 2021;22(17):9247. doi: 10.3390/ijms22179247.
26. Inam H, Sprio S, Tavoni M, Abbas Z, Pupilli F, Tampieri A. Magnetic hydroxyapatite nanoparticles in regenerative medicine and nanomedicine. Int J Mol Sci. 2024;25(5):2809. doi: 10.3390/ijms25052809.
27. Aicha BB, Gasmi S, Lakroun Z, Rouabhi R, Fetoui H, Kebieche M. Cellular and subcellular effects of chronic low-dose Lambda-cyhalothrin pesticide exposure modulated by medicinal plant methanol extract in rat. Mol Cell Biomech. 2024;21:145. doi: 10.62617/mcb.v21.145.
28. Mohideen K, Chandrasekar K, Ramsridhar S, Rajkumar C, Ghosh S, Dhungel S. Assessment of oxidative stress by the estimation of lipid peroxidation marker Malondialdehyde (MDA) in patients with chronic periodontitis: a systematic review and meta-analysis. Int J Dent. 2023;2023(1):6014706. doi: 10.1155/2023/6014706.
29. Timchenko PE, Timchenko EV, Pisareva EV, Vlasov MY, Red'Kin NA, Frolov OO. Spectral analysis of allogeneic hydroxyapatite powders. J PhysConf Ser. 2017;784(1):012060. doi: 10.1088/1742-6596/784/1/012060.
30. Mariappan G, Sundaraganesan N, Manoharan S. The spectroscopic properties of anticancer drug Apigenin investigated by using DFT calculations, FT-IR, FT-Raman and NMR analysis. Spectrochim Acta Mol Biomol Spectrosc. 2012;95:86-99. doi: 10.1016/j.saa.2012.04.089.
31. Xia H, Wang Q. Ultrasonic irradiation: a novel approach to prepare conductive polyaniline/nanocrystalline titanium oxide composites. Chem Mater. 2002;14(5):2158-65. doi: 10.1021/cm0109591.
32. Shahwan M, Anwar S, Yadav DK, Khan MS, Shamsi A. Experimental and computational insights into the molecular interactions between human transferrin and apigenin: implications of natural compounds in targeting neuroinflammation. ACS Omega. 2023;8(49):46967-76. doi: 10.1021/acsomega.3c06799.
33. Sysak S, Czarczynska-Goslinska B, Szyk P, Koczorowski T, Mlynarczyk DT, Szczolko W, *et al*. Metal nanoparticle-flavonoid connections: synthesis, physicochemical and biological properties, as well as potential applications in medicine. Nanomaterials. 2023;13(9):1531. doi: 10.3390/nano13091531.
34. Mahdavi Jafari M, Khayati GR. Prediction of hydroxyapatite crystallite size prepared by sol-gel route: gene expression programming approach. J Sol-Gel Sci Technol. 2018;86(1):112-25. doi: 10.1007/s10971-018-4601-6.
35. Tang S, Shen Y, Jiang L, Zhang Y. Surface Modification of nano-hydroxyapatite/polymer composite for bone tissue repair applications: A Review. Polymers. 2024;16(9):1263. doi: 10.3390/polym16091263.
36. Manzoor H, Arshad N, Qureshi MA, Javed A. Hydroxyapatite-reinforced pectin hydrogel films PEC/PVA/APTES/HAp: doxycycline loading for sustained drug release and wound healing applications. RSC Adv. 2025;15(37):30026-45. doi: 10.1039/d5ra01989c.
37. Remya NS, Syama S, Gayathri V, Varma HK, Mohanan PV. An in vitro study on the interaction of hydroxyapatite nanoparticles and bone marrow mesenchymal stem cells for assessing the toxicological behaviour. Colloid Surf Biointerfaces. 2014;117:389-97. doi: 10.1016/j.colsurfb.2014.02.004.
38. Zhou Z, Zhang Y, Lin L, Zhou J. Apigenin suppresses the apoptosis of H9C2 rat cardiomyocytes subjected to myocardial ischemia-reperfusion injury via upregulation of the PI3K/Akt pathway. Mol Med Rep. 2018;18(2):1560-70. doi: 10.3892/mmr.2018.9115.
39. Zare MF, Rakhshan K, Aboutaleb N, Nikbakht F, Naderi N, Bakhshesh M, *et al*. Apigenin attenuates doxorubicin induced cardiotoxicity via reducing oxidative stress and apoptosis in male rats. Life Sci. 2019;232:116623. doi: 10.1016/j.lfs.2019.116623.

40. Siddiquee R, Mahmood T, Ansari VA, Ahsan F, Bano S, Ahmad S, *et al*. Cardioprotective effect of apigenin and carvedilol against isoproterenol-induced myocardial infarction in rats. Drug Chem Toxicol. 2025:1-7. doi: 10.1080/01480545.2025.2565350.
41. Raberi VS, Esmati M, Bodagh H, Ghasemi R, Ghazal M, Matinpour A, *et al*. The Functionality of Apigenin as a Novel Cardioprotective Nutraceutical with Emphasize on Regulating Cardiac Micro RNAs:-. Galen Med J. 2022;11:e2535. doi: 10.31661/gmj.v11i.2535.
42. Ozyurek M, Gungor N, Baki S, Guclu K, Apak R. Development of a silver nanoparticle-based method for the antioxidant capacity measurement of polyphenols. Anal Chem. 2012;84(18):8052-9. doi: 10.1021/ac301925b.
43. Sharifiaghdam Z, Amini SM, Dalouchi F, Behrooz AB, Azizi Y. Apigenin-coated gold nanoparticles as a cardioprotective strategy against doxorubicin-induced cardiotoxicity in male rats via reducing apoptosis. Heliyon. 2023;9(3). doi: 10.1016/j.heliyon.2023.e14024.
44. Thangaiyan R, Robert BM, Arjunan S, Govindasamy K, Nagarajan RP. Preventive effect of apigenin against isoproterenol-induced apoptosis in cardiomyoblasts. J Biochem Mol Toxicol. 2018;32(11):e22213. doi: 10.1002/jbt.22213.
45. Telange DR, Patil AT, Pethe AM, Fegade H, Anand S, Dave VS. Formulation and characterization of an apigenin-phospholipid phytosome (APLC) for improved solubility, *in vivo* bioavailability, and antioxidant potential. Eur J Pharm Sci. 2017;108:36-49. doi: 10.1016/j.ejps.2016.12.009.
46. Liu HJ, Fan YL, Liao HH, Liu Y, Chen S, Ma ZG, *et al*. Apigenin alleviates STZ-induced diabetic cardiomyopathy. Mol Cell Biochem. 2017;428(1):9-21. doi: 10.1007/s11010-016-2913-9.
47. Wallig MA, Janovitz EB. Morphologic manifestations of toxic cell injury. In Haschek and Rousseaux's Handbook of Toxicologic Pathology. 2013;77-105. doi: 10.1016/B978-0-12-415759-0.00004-2.
48. Adnan HO, Mohammed IA. Cell Cycle-Apoptosis, Similar and Different Aspects. Alex J Vet Sci. 2025;86. doi:10.5455/ajvs.251661.
49. Wu L, Li Y, Liao S, Song Y, Li Y, Li J, *et al*. Modulating Macrophage Polarization for Severe Acute Pancreatitis Therapy via Cisplatin-like Prussian Blue Nanozymes. Theranostics. 2025;15(17):8916-34. doi: 10.7150/thno.113523.
50. Huang M, Bargues-Carot A, Riaz Z, Wickham H, Zenitsky G, Jin H, *et al*. Impact of environmental risk factors on mitochondrial dysfunction, neuroinflammation, protein misfolding, and oxidative stress in the etiopathogenesis of Parkinson's disease. Int J Mol Sci. 2022;23(18):10808. doi: 10.3390/ijms231810808.
51. Jung WW. Protective effect of apigenin against oxidative stress-induced damage in osteoblastic cells. Int J Mol Med. 2014;33(5):1327-34. doi: 10.3892/ijmm.2014.1666.
52. Kwon JW, Kwon HK, Shin HJ, Choi YM, Anwar MA, Choi S. Activating transcription factor 3 represses inflammatory responses by binding to the p65 subunit of NF-κB. Sci Rep. 2015;5(1):14470. doi: 10.1038/srep14470.
53. Nguyen T, Nioi P, Pickett CB. The Nrf2-antioxidant response element signaling pathway and its activation by oxidative stress. J Biol Chem. 2009;284(20):13291-5. doi: 10.1074/jbc.R900010200.

Cite this article: Makeen H, Albratty M. Cardioprotective Effect of Apigenin-Hydroxyapatite Nanocomposite against H_2O_2-Induced Injury in Cardiomyoblast Cells. Indian J of Pharmaceutical Education and Research. 2026;60(3s):s1070-s1086.